Electronic Supplementary Material (ESI) for Inorganic Chemistry Frontiers.
This journal is © the Partner Organisations 2022

# Electronic Supplementary Information

## Experimental Section

**Materials:** Sodium hydroxide (NaOH), hydrochloric acid (HCl), ruthenium(III) chloride trihydrate ($RuCl_3 \cdot 3H_2O$, 98.0%) and ethanol ($C_2H_5OH$) were bought from Beijing Chemical Corporation. (China). Pt/C (20 wt% Pt) was purchased from Alfa Aesar (China) Chemicals Co. Ltd. Nafion (5 wt%) was purchased from Aladdin Reagent (Shanghai, China). Titanium plate (thickness is 0.2 mm) was purchased from Qingyuan Metal Materials Co., Ltd (Xingtai, China) and treated with 3 M HCl for 30 minutes before hydrothermal reaction. All reagents used in this work were analytical grade without further purification.

**Preparation of $RuO_2$@$TiO_2$/Ti:** Firstly, Ti plate (2.0 × 4.0 $cm^2$) was cleaned by ultrasonication in acetone, ethanol, and water for 15 min, respectively. The pretreated Ti plate was put into a 50 mL of Teflon-lined autoclave containing 40 mL of 5 M NaOH solution, then the autoclave was kept in an electric oven at 180 ℃ for 24 h. After the autoclave was cooled down naturally to room temperature, the sample was moved out, washed with deionized water and ethanol several times and dried at 60 ℃ for 30 min. Then the sample was immersed in 0.1 M $RuCl_3 \cdot 3H_2O$ for 4 h in order to exchange $Na^+$ with $Ru^{3+}$. As-prepared Ru-titanate/TP was rinsed with deionized water and ethanol several times, and dried at 60 ℃ for 30 min. Subsequently, Ru-titanate/TP was annealed in a tube furnace at 500 ℃ under an air atmosphere for 2 h. After cooling to room temperature, $RuO_2$@$TiO_2$/TP was finally obtained.

**Preparation of $TiO_2$/Ti:** $TiO_2$/TP was synthesized using the same methods but with 1 M HCl for ion-exchange. As-prepared $H_2Ti_2O_5 \cdot H_2O$/TP was then washed with DI water and ethanol several times and dried at 60 ℃ for 30 min. Subsequently, $H_2Ti_2O_5 \cdot H_2O$/TP was annealed in a tubular furnace at 500 ℃ under an air atmosphere for 2 h. After cooling to room temperature, $TiO_2$/TP was finally obtained.

**Characterizations:** XRD data were acquired from a LabX XRD-6100 X-ray diffractometer with a Cu Kα radiation (40 kV, 30 mA) of wavelength 0.154 nm

(SHIMADZU, Japan). SEM images were collected on a GeminiSEM 300 scanning electron microscope (ZEISS, Germany) at an accelerating voltage of 5 kV. TEM images were acquired on a HITACHI H-8100 electron microscopy (Hitachi, Tokyo, Japan) operated at 200 kV. XPS measurements were performed on an ESCALABMK II X-ray photoelectron spectrometer using Mg as the exciting source.

**Electrochemical measurements:** All electrochemical measurements were carried out on a 660E electrochemical workstation (Chenhua, Shanghai). A conventional one-component three-electrode cell was used. The $RuO_2$@$TiO_2$/TP, $RuO_2$/TP, $TiO_2$/TP, Pt/C on the TP, and bare Ti plate were used as the working electrode, a saturated calomel electrode (SCE) used as the reference electrode, and graphite rode used as the counter electrode, respectively. The geometric surface area of the tested working electrode is 0.5 cm × 0.5 cm. The average loading of $RuO_2$ is about 1.08 mg $cm^{-2}$. In all measurements, SCE was calibrated with respect to RHE. In 0.5 M $H_2SO_4$, E (RHE) = E (SCE) + 0.241 V. In 1.0 M KOH, E (RHE) = E (SCE) + 1.068 V. In 1.0 M PBS, E (RHE) = E (SCE) + 0.655 V. The *i*R-corrected was applied in LSV experiments. ECSA was measured by CV at the potential window from −0.16 to −0.07 V, with different scan rates of 10, 20, 40, 60, and 80 mV $s^{-1}$. The double layer capacitance ($C_{dl}$) was estimated by plotting the $\Delta j = (j_a - j_c)/2$ at −0.115 V against the scan rates, in which the $j_a$ and $j_c$ were the anodic and cathodic current density, respectively. The slope is that of the $C_{dl}$ value. $C_{dl}$ was used to represent the ECSA.

**DFT calculations details:** The Vienna Ab Initio Simulation Package (VASP) code,[1,2] was adopted for all spin-polarized DFT computations, in which the electron and ion interactions were described by the projector augmented wave (PAW) potential.[3,4] The Perdew, Burke, and Ernzerhof (PBE) functional within the generalized gradient approximation (GGA) was adopted for the exchange–correlation interactions.[5] The empirical correction in Grimme's scheme (DFT+D3) method was used to describe the van der Waals (vdW) interactions for reactants or intermediates and catalysts.[6] We constructed the theoretical models of $RuO_2$ (110), $TiO_2$ (101), and $RuO_2$@$TiO_2$

heterostructure with the vacuum space of 25 Å. The cut-off energy for the plane-wave basis set was set to 500 eV with an energy precision of $10^{-5}$ eV and the Brillouin zone was built by 3 × 3 × 1 special k-points based on the Monkhorst Pack scheme for structural configuration optimizations. The free energy profiles, which are efficient in estimating the performance of electrocatalytic reactions, were determined by applying the computational electrode model.[7,8] The Gibbs free energies of hydrogen adsorption ($\Delta G_{H*}$) were calculated as follow:

$$\Delta G_{H*} = \Delta E_{H*} + \Delta E_{ZPE} - T\Delta S$$

In general, the contributions from catalyst substrate to $\Delta S_H$ is very small and negligible, which is thus obtained by $\Delta S_H \approx -1/2 S_{H2}$, $\Delta E_{ZPE} - T\Delta S_H$ is set at 0.24 eV. Thus, $\Delta G_H$ can be rewritten as: $\Delta G_H = \Delta E_H + 0.24$ eV.

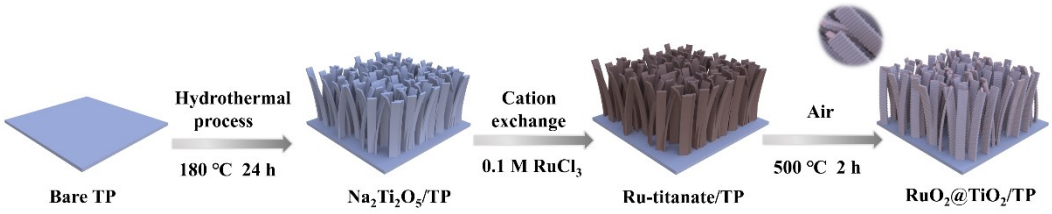


**Fig. S1.** Schematic illustration of the preparation process of $RuO_2$@$TiO_2$/TP.

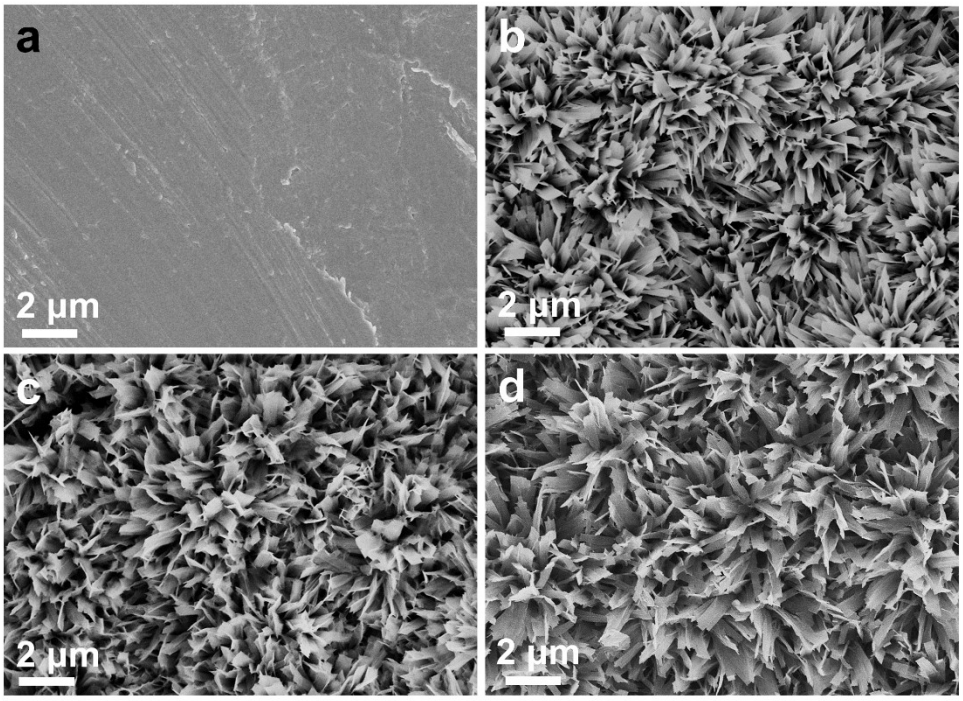


**Fig. S2.** SEM images of (a) bare TP, (b) $Na_2Ti_2O_5$/TP, (c) Ru-titanate/TP, and (d) $TiO_2$/TP.

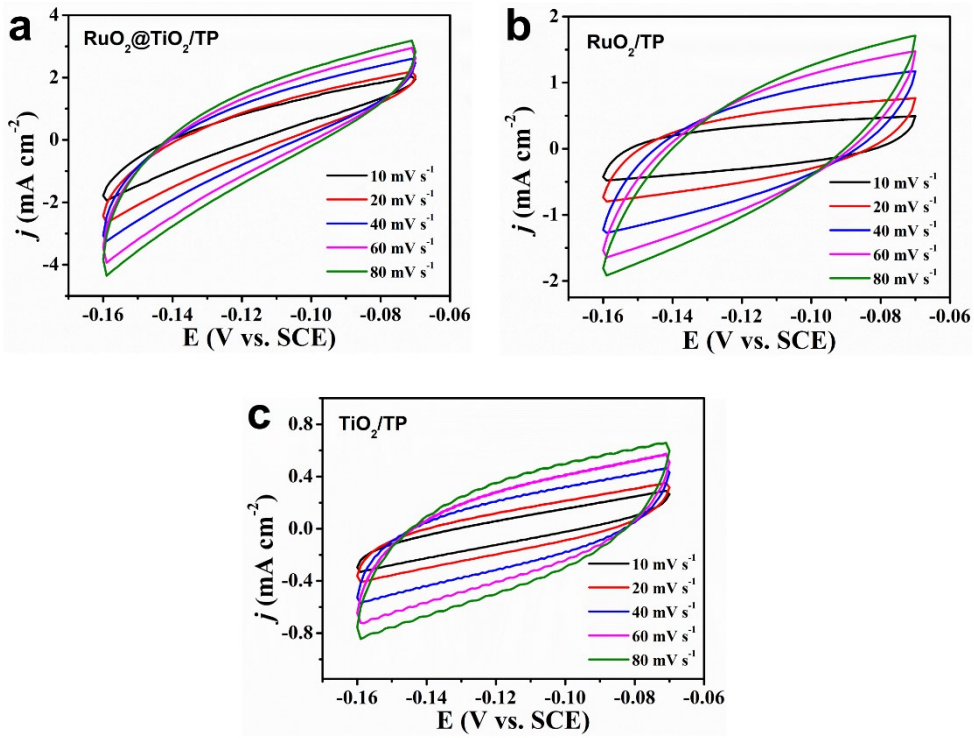


**Fig. S3.** CVs recorded at a series of scan rates for (a) $RuO_2$@$TiO_2$/TP, (b) $RuO_2$/TP, and (c) $TiO_2$/TP.

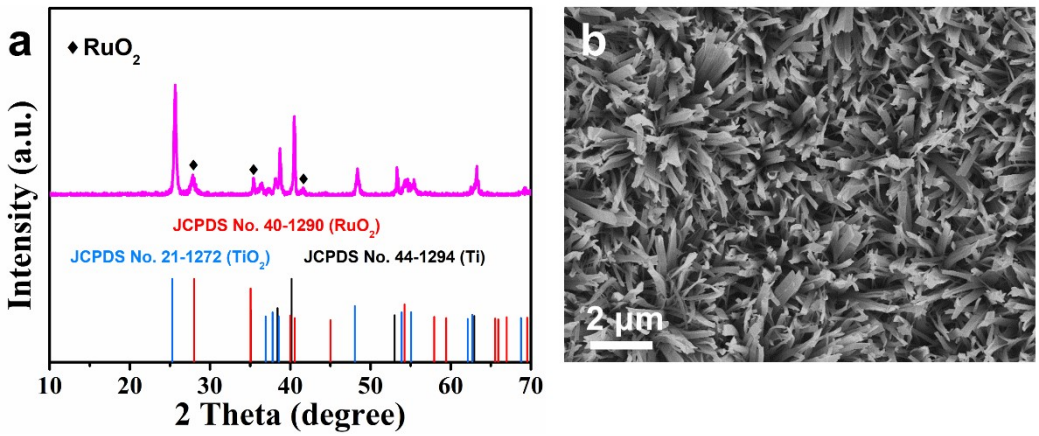


**Fig. S4.** (a) XRD pattern and (b) SEM image of $RuO_2$@$TiO_2$/TP after durability test in 0.5 M $H_2SO_4$.

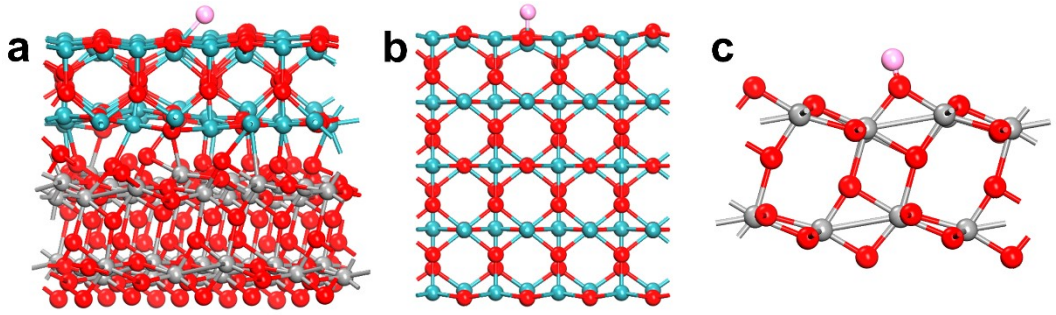


**Fig. S5.** The corresponding atomic structures of H adsorption on (a) $RuO_2$@$TiO_2$, (b) $RuO_2$, and (c) $TiO_2$ surfaces. cyan, red, gray and pink spheres denote the Ru, O, Ti, and H atoms, respectively.

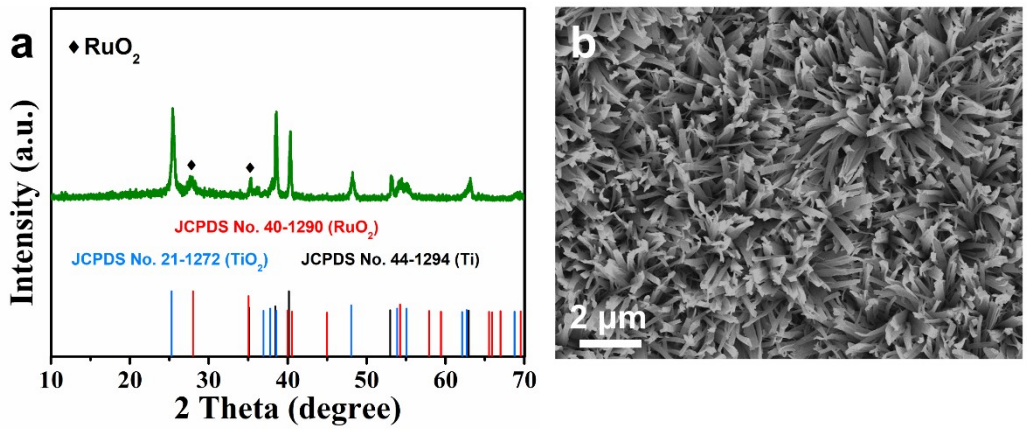


**Fig. S6.** (a) XRD pattern and (b) SEM image of $RuO_2$@$TiO_2$/TP after durability test in 1.0 M KOH.

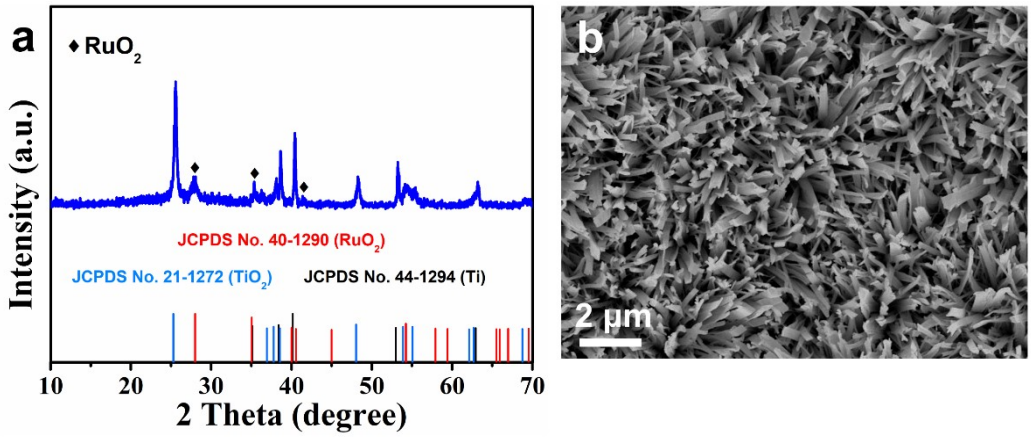


**Fig. S7.** (a) XRD pattern and (b) SEM image of $RuO_2$@$TiO_2$/TP after durability test in 1.0 M PBS.

**Table S1.** Comparison of the HER performance for $RuO_2$@$TiO_2$/TP with other reported catalysts in 0.5 M $H_2SO_4$ solution.

| Electrocatalyst | $\eta_{100}$ (mV) | Stability (h) | Reference |
|---|---|---|---|
| $RuO_2$@$TiO_2$/TP | 130 | 24 | This work |
| $Ni_2P$ nanoparticles | 180 | 20 | 9 |
| WON@NC NAs/CC | 172 | 30 | 10 |
| $MoS_2$/graphene/Ni foam | 263 | / | 11 |
| CoP/CC | 204 | 24 | 12 |
| RuSA-N-$Ti_3C_2T_x$ | ~150 | 12 | 13 |
| $CoSe_2$ NP/CP | 184 | 60 | 14 |
| $NiSe_2$ NP/CP | 206 | / | 14 |

*$\eta_{100}$ represent the overpotentials required to attain $j$ of 100 mA $cm^{-2}$.

**Table S2.** Comparison of the HER performance for $RuO_2$@$TiO_2$/TP with other reported catalysts in 1.0 M KOH solution.

| Electrocatalyst | $\eta_{100}$ (mV) | Stability (h) | Reference |
|---|---|---|---|
| $RuO_2$@$TiO_2$/TP | 143 | 24 | This work |
| Ru-NiFe-P | ~200 | 24 | 15 |
| HC-$MoS_2$/$Mo_2C$ | 354 | 24 | 16 |
| $Ru(OH)_x$/Ag/NF | 103.2 | 10 | 17 |
| 1D-Cu@Co-CoO/Rh | 230 | 14 | 18 |
| $Co_2P$/$Ni_2P$ | ~120 | 10 | 19 |
| Cu-doped Ru/$RuO_2$ | 170 | 11 | 20 |
| NiNS | 197 | 12 | 21 |
| $MoS_2$–$CoS_2$@PCMT | 300 | 20 | 22 |

*$\eta_{100}$ represent the overpotentials required to attain $j$ of 100 mA $cm^{-2}$.

**Table S3.** Comparison of the HER performance for $RuO_2$@$TiO_2$/TP with other reported catalysts in 1.0 M PBS solution.

| Electrocatalyst | $\eta_{50}$ (mV) | Stability (h) | Reference |
|---|---|---|---|
| $RuO_2$@$TiO_2$/TP | 289 | 24 | This work |
| CoP/CC | ~300 | / | 12 |
| CS-PdPt | ~405 | 24 | 23 |
| Re particles | ~400 | 24 | 24 |
| Re@MXene | ~350 | 24 | 24 |
| Re NCs@rGO | ~300 | 24 | 24 |

*$\eta_{50}$ represent the overpotentials required to attain $j$ of 50 mA $cm^{-2}$.

## References


1 G. Kresse and J. Hafner, Ab. initio molecular dynamics for liquid metals, *Phys. Rev. B*, 1993, **47**, 558.

2 G. Kresse and J. Furthmüller, Efficient iterative schemes for ab initio total-energy calculations using a plane-wave basis set, *Phys. Rev. B*, 1996, **54**, 11169.

3 P. E. Blochl, Projector augmented-wave method, *Phys. Rev. B*, 1994, **50**, 17953.

4 G. Kresse and D. Joubert, From ultrasoft pseudopotentials to the projector augmented-wave method, *Phys. Rev. B*, 1999, **59**, 1758.

5 J. P. Perdew, K. Burke and M. Ernzerhof, Generalized gradient approximation made simple, *Phys. Rev. Lett.*, 1996, **77**, 3865.

6 S. Grimme, Semiempirical GGA-Type density functional constructed with a long-range dispersion correction, *J. Comput. Chem.*, 2006, **27**, 1787−1799.

7 J. K. Nørskov, J. Rossmeisl, A. Logadottir and L. Lindqvist, Origin of the overpotential for oxygen reduction at a fuel-cell cathode, *J. Phys. Chem. B*, 2004, **108**, 17886−17892.

8 A. A. Peterson, F. Abild-Pedesen, F. Studt, J. Rossmeisl and J. K. Nørskov, How copper catalyzes the electroreduction of carbon dioxide into hydrocarbon fuels, *Energy Environ. Sci.*, 2010, **3**, 1311−1315.

9 E. J. Popczun, J. R. Mckone, C. G. Read, A. J. Biacchi, A. M. Wiltrout, N. S. Lewis and R. E. Schaak, Nanostructured nickel phosphide as an electrocatalyst for the hydrogen evolution reaction, *J. Am. Chem. Soc.*, 2013, **135**, 9267−9270.

10 Q. Li, W. Cui, J. Tian, Z. Xing, Q. Liu, W. Xing, A. M. Asiri and X. Sun, N-doped carbon-coated tungsten oxynitride nanowire arrays for highly efficient electrochemical hydrogen evolution, *ChemSusChem*, 2015, **8**, 2487–2491.

11 Y. Chang, C. Lin, T. Chen, C. Hsu, Y. Lee, W. Zhang, K. Wei and L. Li, Highly efficient electrocatalytic hydrogen production by $MoS_x$ grown on graphene-protected 3D Ni foams, *Adv. Mater.*, 2013, **25**, 756–760.

12 J. Tian, Q. Liu, A. M. Asiri and X. Sun, Self-supported nanoporous cobalt

phosphide nanowire arrays: an efficient 3D hydrogen-evolving cathode over the wide range of pH 0−14, *J. Am. Chem. Soc.*, 2014, **136**, 7587−7590.

13 H. Liu, Z. Hu, Q. Liu, P. Sun, Y. Wang, S. Chou, Z. Hu and Z. Zhang, Single-atom Ru anchored in nitrogen-doped MXene ($Ti_3C_2T_x$) as an efficient catalyst for the hydrogen evolution reaction at all pH values, *J. Mater. Chem. A*, 2020, **8**, 24710–24717.

14 D. Kong, H. Wang, Z. Lu and Y. Cui, $CoSe_2$ nanoparticles grown on carbon fiber paper: an efficient and stable electrocatalyst for hydrogen evolution reaction, *J. Am. Chem. Soc.*, 2014, **136**, 4897−4900.

15 M. Qu, Y. Jiang, M. Yang, S. Liu, Q. Guo, W. Shen, M. Li and R. He, Regulating electron density of NiFe-P nanosheets electrocatalysts by a trifle of Ru for high-efficient overall water splitting, *Appl. Cataly. B: Environ.*, 2020, **263**, 118324.

16 C. Zhang, Y. Luo, J. Tan, Q. Yu, F. Yang, Z. Zhang, L. Yang, H. Cheng and B. Liu, High-throughput production of cheap mineral-based two-dimensional electrocatalysts for high-current-density hydrogen evolution, *Nat. Commun.*, 2020, **11**, 3724.

17 X. Zhang, B. Guo, F. Li, B. Dong, J. Zhang, X. Ma, J. Xie, M. Yang, Y. Chai and C. Liu, In situ electro-oxidation modulation of $Ru(OH)_x$/Ag supported on nickel foam for efficient hydrogen evolution reaction in alkaline media, *Int. J. Hydrogen Energy*, 2019, **44**, 21683−21691.

18 P. K. L. Tran, D. T. Tran, D. Malhotra, S. Prabhakaran, D. H. Kim, N. H. Kim and J. H. Lee, Highly effective freshwater and seawater electrolysis enabled by atomic Rh-modulated Co-CoO lateral heterostructures, *Small*, 2021, **17**, 2103826.

19 D. Li, L. Liao, H. Zhou, Y. Zhao, F. Cai, J. Zeng, F. Liu, H. Wu, D. Tang and F. Yu, Highly active non-noble electrocatalyst from $Co_2P$/$Ni_2P$ nanohybrids for pH-universal hydrogen evolution reaction, *Mater. Today Phy.*, 2021, **16**, 100314.

20 K. Yang, P. Xu, Z. Lin, Y. Yang, P. Jiang, C. Wang, S. Liu, S. Gong, L. Hu and Q. Chen, Ultrasmall Ru/Cu-doped $RuO_2$ complex embedded in amorphous

carbon skeleton as highly active bifunctional electrocatalysts for overall water splitting, *Small*, 2018, **14**, 1803009.

21 Y. Zhao, B. Jin, A. Vasileff, Y. Jiao and S. Qiao, Interfacial nickel nitride/sulfide as a bifunctional electrode for highly efficient overall water/seawater electrolysis, *J. Mater. Chem. A*, 2019, **7**, 8117–8121.

22 J. Yang, C. Chai, C. Jiang, L. Liu and J. Xi, $MoS_2$–$CoS_2$ heteronanosheet arrays coated on porous carbon microtube, *J. Power Sources*, 2021, **514**, 230580.

23 B. T. Jebaslinhepzybai, N. Prabu and M. Sasidharan, Facile galvanic replacement method for porous Pd@Pt nanoparticles as an efficient HER electrocatalyst, *Int. J. Hydrogen Energy*, 2020, **45**, 11127−11137.

24 S. Xu, H. Li, J. Lee, N. C. S. Selvam, B. Kang, J. Y. Lee and P. J. Yoo, Re nanoclusters anchored on nanosheet supports: formation of Re-O-matrix bonding and evaluation as all-pH-range hydrogen evolution reaction (HER) electrocatalysts, *J. Energy Chem.*, 2022, **69**, 185−193.